Since January 2020 Elsevier has created a COVID-19 resource centre with free information in English and Mandarin on the novel coronavirus COVID-19. The COVID-19 resource centre is hosted on Elsevier Connect, the company's public news and information website.

Biomedical Signal Processing and Control 75 (2022) 103627

Contents lists available at ScienceDirect

Biomedical Signal Processing and Control

journal homepage: www.elsevier.com/locate/bspc

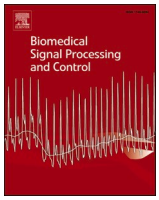

New pulse oximetry detection based on the light absorbance ratio as determined from amplitude modulation indexes in the time and frequency domains

Pattana Kainan [a,*], Ananta Sinchai [b], Panwit Tuwanut [c], Paramote Wardkein [a]

[a] Department of Telecommunication Engineering, King Mongkut's Institute of Technology Ladkrabang, Ladkrabang, Bangkok 10520, Thailand
[b] College of Advanced Manufacturing Innovation, King Mongkut's Institute of Technology Ladkrabang, Bangkok 10520, Thailand
[c] Faculty of Information Technology, King Mongkut's Institute of Technology Ladkrabang, Ladkrabang, Bangkok 10520, Thailand

ARTICLE INFO

Keywords:
Pulse oximetry
Photoplethysmography
Light absorbance ratio
Motion artifact
Amplitude modulation
Frequency-division multiplexing

ABSTRACT

The Pandemic COVID-19 situation, a pulse Oximetry is significant to detect a varying blood oxygen saturation of a patient who needed the device to operate with continuous, rapid, high accuracy, and immune of moving artifacts. In this article, three main schemes for low-complexity pulse oximetry detection are proposed. In the first scheme, the light absorbance ratio (R) is obtained by separating the red and infrared photoplethysmography (PPG) amplitude modulation (AM) signals from the frequency-division multiplexing (FDM) signal with two different bandpass filters (BPFs), determining the ratio of modulation index of red and infrared PPG AM signals. In the second scheme, the output PPG AM signals for the red and infrared light wavelengths from the BPFs are transformed into the frequency domain such that the AC components of both PPG AM signals are the magnitudes of the highest peaks in their respective sidebands, while the DC components are the magnitude of their carrier frequencies; then, the AC/DC ratio of the red PPG AM signal is divided by the AC/DC ratio of the infrared PPG AM signal is R. In the last scheme, the FDM signal is transformed into the frequency domain without being passed through any BPF, and R is obtained in the same way as in the same second scheme. Experimental results obtained by using the first scheme have an average error of about 0.7138%, for the second and the last scheme have an average error of about 1%, and all the methods agree with the corresponding mathematical model.

1. Introduction

Arterial blood oxygen saturation (SaO_2) is an important vital sign of the human body. It is the proportion of the measured oxyhaemoglobin (HbO_2) concentration relative to the total haemoglobin concentration in the blood. Currently,SaO_2 can be assessed by using a technique named pulse oximetry. Pulse oximetry yields an empirical measurement of SaO_2 called pulse oxygen saturation (SpO_2). UnlikeSaO_2, SpO_2 is based on only two functional haemoglobins, namely, HbO_2 and deoxyhaemoglobin (Hb). These haemoglobins can reversibly bind with oxygen molecules. Generally, the types of haemoglobins present in a healthy person are functional haemoglobins, so SpO_2 can be considered approximately equal to SaO_2 if SaO_2 is greater than 70% [1–4]. The pulse oximetry technique does not require a blood sample from the patient, causes no pain and is easy to perform. Traditional pulse oximetry relies on a pulse oximetry probe with dual light sources and a single light detector attached to the fingertip or earlobe [5]. This technique is based on the principle of the Beer-Lambert law [6–7]. Therefore, before any device for measuring SpO_2 using an optical process could be invented, various chemical processes were first proposed, such as Van Slyke's method, the mixing syringe method, and methods using the principle of oxidation, for example, the Clark electrode and the galvanic electrode [8–11]. However, chemical processes require chemical expertise, and any such process requires a blood sample from the patient, which must first be sampled from the patient's body.

In addition to chemical processes, there are also various optical processes available for measurement purposes. One of these optical processes is spectrophotometry, which is the basis of the technique known as oximetry. Oximetry refers to a method of measuring SaO_2 using optical techniques, and pulse oximetry is one important oximetry technique. Almost all optical techniques are based on the Beer-Lambert law, especially spectrophotometry, which uses the isosbestic point wavelength to measure SaO_2. At the isosbestic point, the extinction coefficients of both HbO_2 and Hb are identical [12]. Moreover, the CO-

* Corresponding author.

https://doi.org/10.1016/j.bspc.2022.103627
Received 10 July 2021; Received in revised form 18 December 2021; Accepted 5 March 2022
Available online 11 March 2022

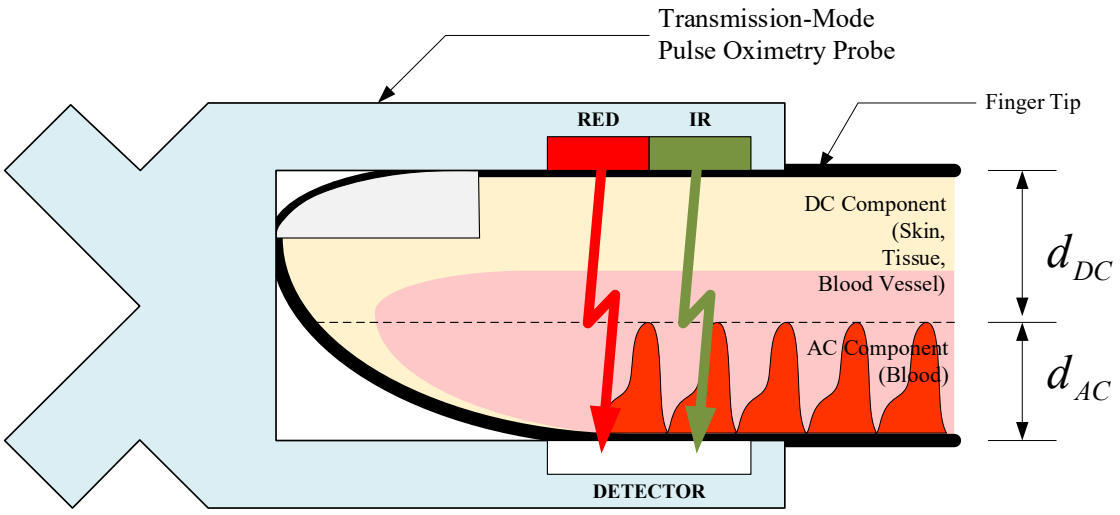

Fig. 1. A transmission-mode pulse oximetry probe. The pulse oximetry probe is attached to the fingertip and emits dual light signals, consisting of red light and infrared light, which pass through the fingertip to a single light detector.

oximeter method has been proposed based on a principle similar to that of spectrophotometry. The difference is that a CO-oximeter can also measure the concentrations of other kinds of haemoglobins, such as methaemoglobin and carboxyhaemoglobin. To measure the concentrations of various kinds of haemoglobins, a CO-oximeter needs to use four light sources of different wavelengths. However, with these two oximeters, a patient's blood sample is still needed to estimate SaO_2.

In the 1930s, non-invasive oximeters were invented, of which Kramer's oximeter was the first example. Kramer's oximeter used a single red light source to measure SaO_2; because the absorbance of blood depends on SaO_2, a single light source can be used for this measurement. At around the same time, Matthes' oximeter was invented. Matthes' oximeter emitted both red and green light, which passed through the earlobe to a photocell. Initially, optical techniques for measuring SaO_2 had no special name; this was true until Glen Milliken established the word "oximetry" [13]. Milliken's oximeter was similar to Matthes' oximeter, with the difference that the two light sources produced red and infrared light. In 1971, Takuo Aoyaki invented an oximeter using a red light source with a 630 nm wavelength and an infrared light source with a 900 nm wavelength. These two wavelengths have now become basis of modern pulse oximeters [14–15]. Moreover, in addition to measuring SpO_2, this oximeter could also measure the heart rate.

SpO_2 is estimated from the light absorbance ratio (R) between the signals measured by the light detector of a pulse oximetry probe, which are called photoplethysmography (PPG) signals. A PPG signal has two components: an AC component and a DC component. The AC component is a pulsatile signal, and the DC component is a non-pulsatile signal. R is calculated as a ratio among the AC and DC components of the red and infrared PPG signals. Therefore, if the PPG signals are interfered, the estimated result for R will be in error. Almost all such interference arises from movements, which cause effects known as motion artefacts (MAs). MAs cause distortion of the PPG signal waveform. To reduce MAs, many methods have been proposed, which can be classified into three main categories: hardware methods, software methods, and methods combining hardware and software features. For example, active noise cancellation using an adaptive filter combined with an accelerometer sensor [16–18] is one such combined hardware and software implementation. Software implementations focus on signal processing methods, such as Fourier series analysis [19], the Fourier transform [20], the wavelet transform [21], and others [22–30]. By means of frequency-domain transformation, a new method of calculating R from the magnitude spectrum becomes available. In the frequency domain, the AC component is the magnitude of the cardiac-frequency signal, and the DC component is the magnitude of the zero-hertz signal. Recently, a method of shifting the frequency band of a PPG signal from a low-frequency location to a higher-frequency location has been proposed [31–33]. These methods use a sinusoidal wave instead of a square wave signal to drive a dual light source. In the past, square wave control signals have been used to drive the dual light source, causing the signals at the light detector to be two pulse amplitude modulated (PAM) signals in the time-division multiplexing (TDM) form; in contrast, under two sinusoidal control signals of different frequencies, the obtained signals are two amplitude modulated signals (AM) of different carrier frequencies, corresponding to frequency-division multiplexing (FDM) [32–33]. To calculate R from such a FDM signal, bandpass filters (BPFs) and demodulators have been used to recover the normal PPG signals and calculate R in either the time domain or the frequency domain as described above.

PPG AM signals have two advantages: the first one is the effects of MAs are decreased [32], and the second one, the modulation index of a PPG AM signal also corresponds to the ratio between the AC and DC components of a conventional PPG signal, which is identical to the light absorbance (A), so, the modulation index is also identical to the light absorbance. Therefore, the ratio between the modulation indexes of the red and infrared PPG AM signals is equal to R. Moreover, the frequency components of the PPG signal are shifted from a low frequency band to a higher frequency band because of the AM effect. In the low frequency band, the ratio between the AC and DC components in the frequency domain is equivalent to the ratio between the magnitude of the cardiac-frequency signal and the magnitude of the zero-hertz signal [20]. Therefore, there is a possibility that the ratio between the AC and DC components in the higher frequency band is similarly equivalent to the ratio between the magnitudes of the shifted cardiac-frequency and carrier-frequency signals. Accordingly, R can be directly calculated from the two PPG AM signals. To calculate R from the PPG AM signals (from either the modulation index ratio or the spectrum ratio), it is unnecessary to first demodulate or recover the conventional PPG signal. Thus, the spectrum of the FDM signal, which is obtained directly from the amplifier circuit, can be used to calculate R without any BPF or demodulator.

Before the results are presented, the theory behind pulse oximetry and AM should be introduced. In the next section, the fundamental background on SpO_2 measurement and AM is presented, and the proposed method are then described, as well as the experimental setup of this article.

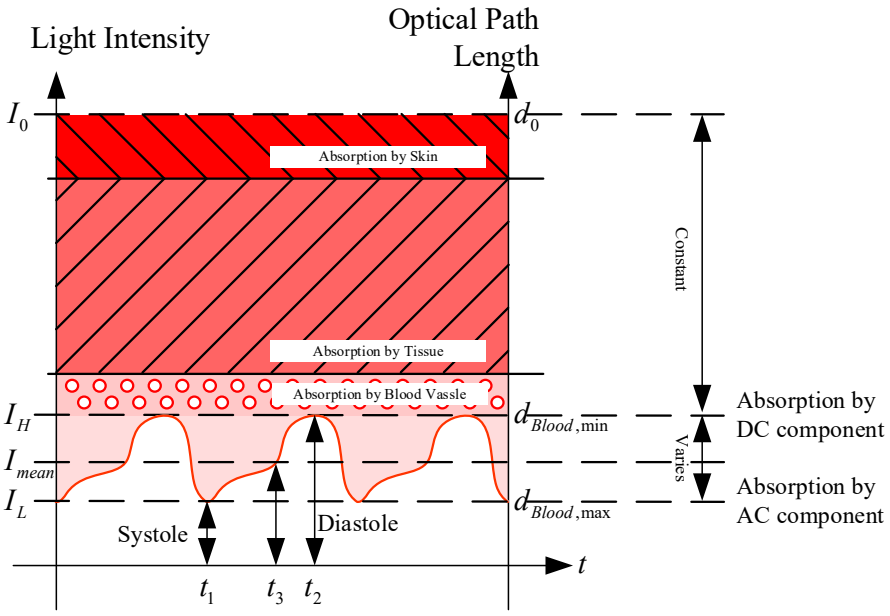

Fig. 2. A PPG signal received at the light detector as represented in the time domain. Here, I_0 is the emitted light intensity; time t_1 corresponds to the systolic phase, in which the optical path length of the blood is the longest ($d_{Blood,max}$) and the light intensity is the lowest (I_L), while time t_2 corresponds to the diastolic phase, in which the optical path length of the blood is the shortest ($d_{Blood,min}$) and the light intensity is the highest (I_H). Time t_3 corresponds to the mean light intensity (I_{mean}).

2. Pulse oxygen saturation measurement

As mentioned before, measuring SpO_2 is a technique for estimating SaO_2 based on the concentrations of Hb and HbO_2. SpO_2 is defined as shown in Eq. (1).

$$SpO_2 = \frac{c_{HbO_2}}{c_{HbO_2} + c_{Hb}} \tag{1}$$

From Eq. (1), if the concentrations of Hb and HbO_2 have known, SpO_2 can be determined easily; however, if SpO_2 is to be determined based on a non-invasive optical technique, both concentrations cannot be directly obtained. Therefore, SpO_2 is indirectly determined as follows. The optical technique for determining SpO_2 is based on the principle of the Beer-Lambert law, which describes the relationship between the emitted light (I_0) and the transmitted light (I) when I_0 is partially absorbed by a homogeneous medium that has an extinction coefficient of $\varepsilon(\lambda)$ at the wavelength λ, a concentration of c, and an optical path length of d. This relationship is shown in Eq. (2).

$$I = I_0 e^{-\varepsilon(\lambda)cd} \tag{2}$$

The absorbance (A) is defined in Eq. (3).

$$A = -ln\frac{I}{I_0} = \varepsilon(\lambda)cd \tag{3}$$

To use a pulse oximeter, as shown in Fig. 1, the probe must be attached to the fingertip; however, a fingertip is not a homogeneous medium. The absorbance of the fingertip (A_{Finger}) can be separated into two components. The first component (A_{DC}) represents the DC absorbance, which is predominantly related to substances such as skin, tissue, and blood vessels, and the second component (A_{AC}) represents the AC absorbance, which is predominantly related to the blood. The extinction coefficient for the DC absorbance component at a wavelength of λ is $\varepsilon_{DC}(\lambda)$, the corresponding concentration is c_{DC}, and the corresponding optical path length is d_{DC}. On the other hand, the extinction coefficient for the AC absorbance component at the same wavelength is $\varepsilon_{AC}(\lambda)$ the corresponding concentration is c_{AC}, and the corresponding optical path length is d_{AC}. So, A_{Finger} can be approximated as a sum of two components, A_{DC} and A_{AC}.

As seen from Fig. 1, A_{AC} is essentially equivalent to the absorbance of the blood (A_{Blood}), which depends on the absorbance of Hb andHbO_2, so A_{Finger} can be expressed as shown in (4).

$$A_{Finger} = A_{DC} + A_{AC} = \varepsilon_{DC}(\lambda)c_{DC}d_{DC} + (\varepsilon_{HbO_2}(\lambda)c_{HbO_2} + \varepsilon_{Hb}(\lambda)c_{Hb})d_{Blood} \tag{4}$$

From Eq. (4), The A_{DC} must be eliminated in order to obtain A_{Blood}. This problem can be solved by determining the difference between the fingertip absorbances at different times. The optical path length d_{Blood} changes over time because of the contraction of the heart, as characterized by the systolic and diastolic phases. In Eq. (4), A_{DC} is typically constant, while A_{AC} varies; therefore, the difference in absorbance between the systolic ($A_{Systole}$) and diastolic ($A_{Diastole}$) phases can be expressed as shown in Eq. (5).

$$A_{Different} = A_{Systole} - A_{Diastole} = (\varepsilon_{HbO_2}(\lambda)c_{HbO_2} + \varepsilon_{Hb}(\lambda)c_{Hb})\Delta d_{Blood} = A_{Blood} \tag{5}$$

Eq. (5) expresses the absorbance of the blood (A_{Blood}), and Δd_{Blood} is the absolute optical path length in the blood. At this point, the concentrations of oxyhaemoglobin and deoxyhaemoglobin are still unknown, and there is also one additional unknown (Δd_{Blood}). This problem can be solved by using two light sources with different wavelengths. The most common wavelengths for pulse oximetry probes are red and infrared wavelengths. To eliminate the effect of Δd_{Blood}, the light absorbance ratio is calculated; because both light signals are travelling through the same finger, the optical path lengths for both wavelengths are equal. The light absorbance ratio (R) is defined as shown in Eq. (6):.

$$R = \frac{(\varepsilon_{HbO_2}(\lambda_{RED})c_{HbO_2} + \varepsilon_{Hb}(\lambda_{RED})c_{Hb})}{\varepsilon_{HbO_2}(\lambda_{IR})c_{HbO_2} + \varepsilon_{Hb}(\lambda_{IR})c_{Hb}} \tag{6}$$

By rearranging Eq. (1) and Eq. (6), SpO_2 can be written as a function of R, as shown in Eq. (7) [7].

$$SpO_2 = \frac{\varepsilon_{Hb}(\lambda_{RED}) - \varepsilon_{Hb}(\lambda_{IR})R}{\varepsilon_{Hb}(\lambda_{RED}) - \varepsilon_{HbO_2}(\lambda_{RED}) + (\varepsilon_{HbO_2}(\lambda_{IR}) - \varepsilon_{Hb}(\lambda_{IR}))R} \tag{7}$$

Eq. (7) shows that it is not necessary to know the concentrations of haemoglobins; instead, SpO_2 can be determined based only on the R-value. Moreover, the extinction coefficients in Eq. (7) are constant at specific wavelengths, so the empirical equation for estimating SpO_2 can be further written as follows [34].

$$SpO_2 = 110 - 25R \tag{8}$$

Theoretically, R is the ratio of A_{Blood} between the red and infrared light signals, but in practise, R can be obtained from the light intensity signal shown in Fig. 2. This signal is called the PPG signal, and R can be calculated from the PPG signal via the following three methods.

2.1. Neighbour minimum valley and maximum peak method (Peak and valley Method)

From the signal in Fig. 2, the light intensities I_H and I_L are expressed as shown in Eqs. (9) and (10), respectively.

$$I_H = I_0 e^{-\varepsilon_{DC}(\lambda)c_{DC}d_{DC}} \tag{9}$$

$$I_L = I_0 e^{-\varepsilon_{DC}(\lambda)c_{DC}d_{DC}} e^{-\varepsilon_{AC}(\lambda)c_{AC}d_{AC}} = I_H e^{-\varepsilon_{AC}(\lambda)c_{AC}d_{AC}} \tag{10}$$

Because I_L is the light intensity due to absorption by the AC component, the corresponding absorbance is given by Eq. (11):

$$-ln\frac{I_L}{I_H} = \varepsilon_{AC}(\lambda)c_{AC}d_{AC} = (\varepsilon_{HbO_2}(\lambda)c_{HbO_2} + \varepsilon_{Hb}(\lambda)c_{Hb})d_{Blood} = A_{Blood} \tag{11}$$

Therefore, R as calculated with the peak and valley method is.

$$\frac{-ln\frac{I_{L,RED}}{I_{H,RED}}}{-ln\frac{I_{L,IR}}{I_{H,IR}}} = \frac{(\varepsilon_{HbO_2}(\lambda_{RED})c_{HbO_2} + \varepsilon_{Hb}(\lambda_{RED})c_{Hb})}{(\varepsilon_{HbO_2}(\lambda_{IR})c_{HbO_2} + \varepsilon_{Hb}(\lambda_{IR})c_{Hb})} = R \tag{12}$$

Eq. (12) shows that in this method, I_0 is discarded, and only I_H and I_L of the PPG signals from the red and infrared wavelength light sources are used to compute R.

2.2. Derivative method

In this technique, R is calculated by separating the DC and AC components. To decrease the potential for confusion among variables, the notation for the optical path length d is changed to L(t) here; then, based on Fig. 2, the derivative of Eq. (2) is written as shown in Eq. (13).

$$\frac{dI(t)}{dt} = -\varepsilon(\lambda)c\frac{dL(t)}{dt}\left(I_0 e^{-\varepsilon(\lambda)cL(t)}\right) = -\varepsilon(\lambda)c\frac{dL(t)}{dt}I(t) \tag{13}$$

Dividing both sides of Eq. (13) by I(t) yields the result shown in Eq. (14):.

$$\frac{\frac{dI(t)}{dt}}{I(t)} = -\varepsilon(\lambda)c\frac{dL(t)}{dt} \tag{14}$$

By comparing Eq. (14) to Eq. (3), the term $\frac{\frac{dI(t)}{dt}}{I(t)}$ can be seen to be the light absorbance, which is equivalent to A_{Blood}; therefore, R can be written in derivative form as shown in Eq. (15).

$$\frac{\frac{dI_{RED}(t)}{dt}}{\frac{I_{RED}(t)}{\frac{dI_{IR}(t)}{dt}}} = \frac{(\varepsilon_{HbO_2}(\lambda_{RED})c_{HbO_2} + \varepsilon_{Hb}(\lambda_{RED})c_{Hb})}{(\varepsilon_{HbO_2}(\lambda_{IR})c_{HbO_2} + \varepsilon_{Hb}(\lambda_{IR})c_{Hb})} = R \tag{15}$$

Through approximation of the derivatives, Eq. (16) is obtained.

$$\frac{dI(t)}{dt} \approx I(t_2) - I(t_1) \tag{16}$$

From Fig. 2, all the light intensities can be substituted into Eq. (15) to obtain Eq. (17):.

$$\frac{\frac{dI_{RED}(t)}{dt}}{\frac{I_{RED}(t)}{\frac{dI_{IR}(t)}{dt}}} = \frac{\frac{I_{RED}(t_2) - I_{RED}(t_1)}{I_{RED}(t_3)}}{\frac{I_{IR}(t_2) - I_{IR}(t_1)}{I_{IR}(t_3)}} = \frac{\frac{AC_{RED}}{DC_{RED}}}{\frac{AC_{IR}}{DC_{IR}}} = R \tag{17}$$

Here, AC_{RED} and DC_{RED} are the light intensities of the AC and DC components of the red light signal, respectively, and AC_{IR} and DC_{IR} are the light intensities of the AC and DC components of the infrared light signal, respectively.

In Eq. (17), the expression for R from the derivative method, the emitted light intensities from the dual light sources are discarded because this method considers only the highest and lowest light intensities to compute R.

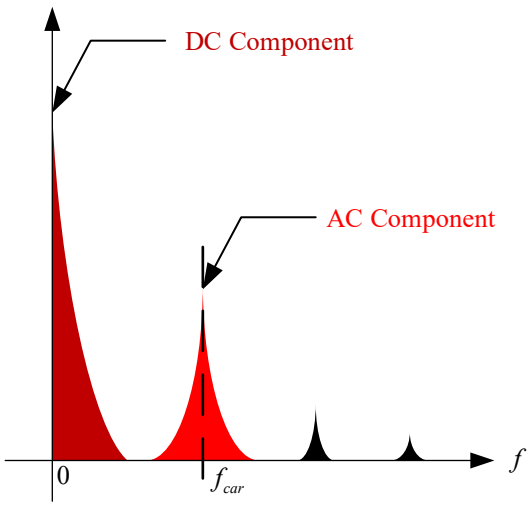

Fig. 3. A PPG signal received at the light detector as represented in the frequency domain.

In the methods presented above, R is calculated based on the measured light intensity at the receiving detector; however, in practise, the light detector in an oximetry probe is a photodiode. In general, a photodiode transforms light intensity into a current, and this current is typically then converted into a voltage by a *trans*-impedance amplifier to simplify signal processing; therefore, the light intensities in Eqs. (12) and (17) can be expressed as voltages. While the two previous methods involve calculating R in the time domain, the last technique presented below instead employs the magnitude spectrum to calculate R in the frequency domain.

2.3. Spectral analysis method

The magnitude spectrum of PPG signal is shown in Fig. 3, In the frequency domain, the AC component is the magnitude of the highest peak in the cardiac-frequency band (f_{car}), while the DC component is the magnitude of the zero-hertz signal. The calculation of R via the spectral analysis method relies on the direct substitution of the DC and AC components into Eq. (17).

From a communication perspective, because a pulse oximetry probe has dual light sources and a single light detector, if both light sources are active simultaneously, the light detector will be unable to separate the red PPG signal from the infrared PPG signal; therefore, TDM is used. Traditionally, the two light sources are controlled by square wave signals with two different phases, and the signals are obtained in PAM form; however, in this article, the two light sources are considered to be controlled by two sinusoidal waves of different frequencies based on Sakkarin's method [32]. The signal pattern obtained at the light detector when the dual light sources are controlled with sinusoidal waves is formed of two AM signals. Therefore, in the next subsection, the fundamentals of the AM technique are described.

3. Amplitude modulation

In telecommunication, AM and frequency modulation (FM) are common modulation techniques used in radio broadcasting. The simplest modulation technique is to vary some parameter of the sinusoidal waveform, such as the amplitude, frequency, or phase, versus the message signal. In this article, the double-sideband suppressed-carrier AM (AM-DSBSC) approach with a large carrier is assumed. Before the use of the above techniques to calculate R for estimating SpO_2 is demonstrated, in this section, basic AM is briefly described.

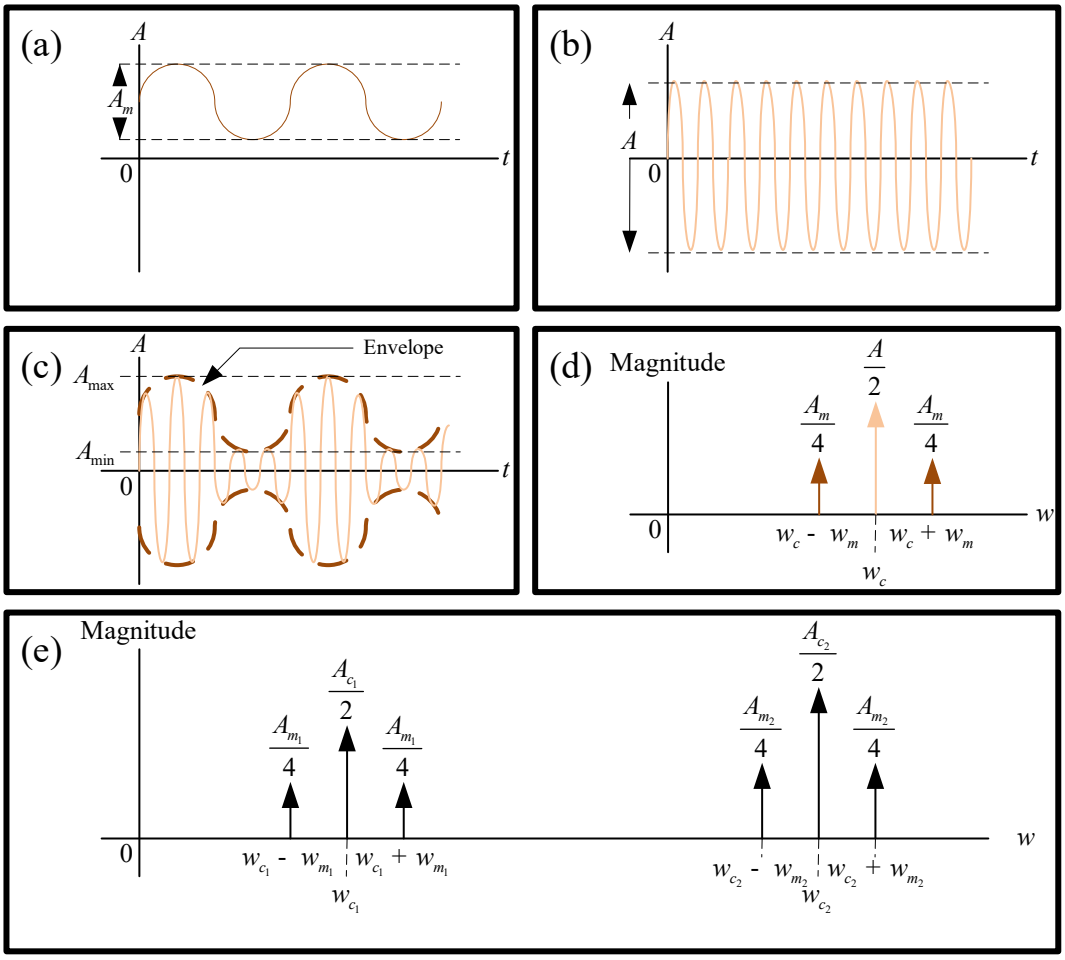

Fig. 4. Amplitude modulation. (a) The message signal (m(t)) is a low-frequency sinusoidal wave with frequency ω_m and amplitudeA_m, i.e., $m(t) = A_m cos(\omega_m t)$. (b) The carrier signal c(t) is a high-frequency sinusoidal wave with frequency ω_c and amplitudeA, i.e., $c(t) = Acos(\omega_c t)$. (c) The AM signal consisting of the message signal $m(t)$ and the carrier signal$c(t)$. (d) The magnitude spectrum of the AM signal (Fig. 4(c)). (e) A FDM signal, which is a combination of two AM signals. The first AM signal's carrier frequency isω_{c_1}, and that of the second AM signal isω_{c_2}.

First, considering the message signal shown in Fig. 4(a) and the carrier signal shown in Fig. 4(b); the corresponding AM signal is described by Eq. (18) and depicted in Fig. 4(c).

$$AM(t) = Acos(\omega_c t) + m(t)cos(\omega_c t) = (A + m(t))cos(\omega_c t) \tag{18}$$

The term $m(t)cos(\omega_c t)$ is the AM-DSBSC signal, and the term $Acos(\omega_c t)$ is the carrier signal when they are combined; thus, Eq. (18) represents an AM-DSBSC signal with a large carrier, which is a well-known type of AM signal. By substituting $m(t) = A_m cos(\omega_m t)$ into Eq. (18) and Eq. (19) is obtained.

$$\boldsymbol{AM}(t) = Acos(\omega_c t) + \frac{A_m}{2}cos((\omega_c - \omega_m)t) + \frac{A_m}{2}cos((\omega_c + \omega_m)t) \tag{19}$$

When Eq. (19) is transformed into the frequency domain, the terms $\omega_c - \omega_m$ and $\omega_c + \omega_m$ are the lower sideband (LSB) and the upper sideband (USB), respectively. The magnitude spectrum of the AM signal is shown in Fig. 4(d).

In addition to the amplitude and frequency of an AM signal, the modulation index (μ) is also an important parameter. From Fig. 4(c), μ can be obtained as shown in Eq. (20).

$$\mu = \frac{A_m}{A} = \frac{A_{max} - A_{min}}{A_{max} + A_{min}} = \frac{|m(t)_{min}|}{A} \tag{20}$$

In the case of many sources of messages wanting to simultaneously send information in the same channel, various different carrier frequencies are allocated to these message sources for modulation, after which the modulated signals are summed together and transmitted through the provided channel. This process is known as the FDM technique. At the receiver site, demodulation cannot be directly performed; instead, the FDM signal must be filtered with a BPF with a centre frequency corresponding to each carrier frequency. After that, the AM detector is used to recover information as mentioned above. Eq. (21) shows the FDM signal obtained by multiplexing two AM signals formed from two message signals ($m_1(t)$ and $m_2(t)$) and carrier signals of two different frequencies (ω_{c_1} and ω_{c_2}).

$$\boldsymbol{FDM}(t) = A_{c_1}cos(\omega_{c_1}t) + m_1(t)cos(\omega_{c_1}t) + A_{c_2}cos(\omega_{c_2}t) + m_2(t)cos(\omega_{c_2}t) \tag{21}$$

The magnitude spectrum of the FDM signal considered in this example is shown in Fig. 4(e).

4. New methods for calculating the light absorbance ratio

Previously, the principles of pulse oximetry and AM were reviewed. The pulse oximetry principle was explained, illustrating why the non-invasive measurement of SpO_2 requires two light sources with two different wavelengths. Finally, the mathematical expression was presented to show that in order to measure SpO_2, it is not necessary to directly measure the concentration of any haemoglobin type in blood. Only the light intensities need to be measured to calculate R in order to estimate SpO_2.

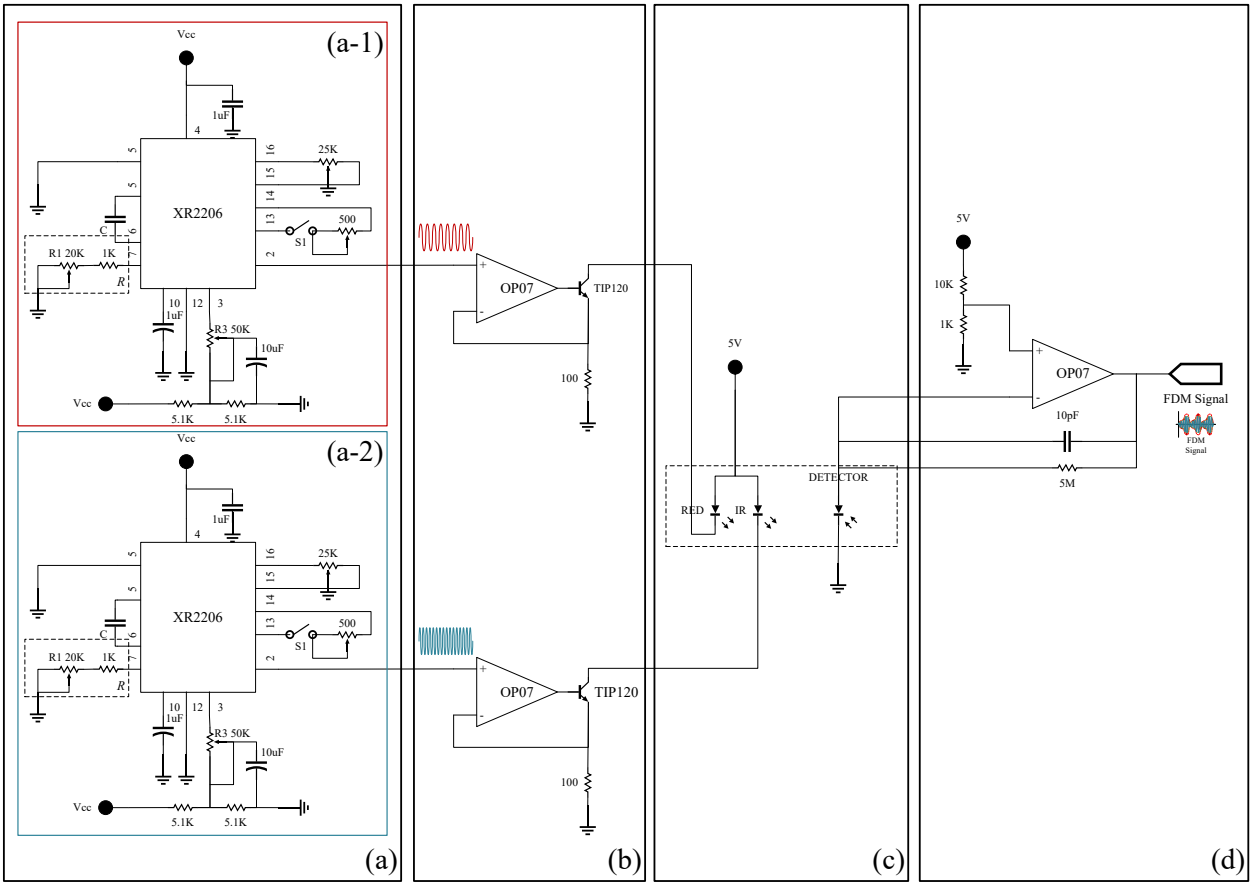

Fig. 5. The analogue front end. (a) The oscillator circuits generate (a-1) a cosine signal with a frequency of 1070 Hz and (a-2) a cosine signal with a frequency of 1550 Hz. (b) LED driver circuits. (c) Datex-Ohmeda's pulse oximetry probe with a common LED anode. (d) Trans-impedance amplifier circuit.

Generally, a pulse oximetry probe includes two light sources and a single light detector. The single light detector needs to detect both light signals separately. Traditionally, the two light sources are driven by two square wave signals with different phases. From a communication point of view, this corresponds to TDM; when the signal from the light detector is considered, these signals are two PAM signals. In Sakkarin's research [32], the control signals were changed from square wave signals to cosine signals. With this method, two cosine signals of different frequencies are used to control the light sources, so the signal received at the light detector is a combination of two PPG AM signals in FDM form. The carrier signals of the two PPG AM signals are the cosine signals used to drive the light sources, and the message signals are the PPG signals. The advantage of controlling the two light sources with two different-frequency cosine signals is that ambient light will not disturb the PPG signals because the frequency bands of the PPG signals are moved to a higher frequency. Sakkarin calculated R by using two BPFs to separate the two PPG AM signals and finally demodulating the PPG AM signals into PPG signals to be processed using the conventional method.

However, when an AM signal is considered in the time domain, its modulation index is equal to the ratio of the amplitude of the message signal to its DC offset. If the message signal is a PPG signal, the modulation index of a PPG AM signals corresponds to the $\frac{AC}{DC}$ ratio of the PPG signal. Meanwhile, T. L. Rusch [20] has explained the method for calculating R in the frequency domain. The PPG AM signals in the frequency domain correspond to T. L. Rusch's method: the AC component is the magnitude of the highest peak in the USB (or LSB) of the PPG AM signal, and the DC component is the magnitude of the peak at its carrier frequency. Finally, the combined signal consisting of the red and infrared PPG AM signals are in FDM form can be used to calculate R in the same way as in the second scheme. With this method, the PPG AM signals do not need to be demodulated to calculate R, and the FDM signal does not need to be filtered by any BPF. Accordingly, this article has proposed two types of novel methods for calculating R: in the time domain and in the frequency domain.

4.1. Calculation of R in the time domain

As mentioned above, R can be determined from Eq. (17). When considering the modulation index in Eq. (20), so, the term $\frac{A_{max}-A_{min}}{2}$ is the AC component of the PPG signal and the term $\frac{A_{max}+A_{min}}{2}$ is the DC component of the PPG signal, or the average of the PPG signal; thus, μ_{PPG} is the $\frac{AC}{DC}$ ratio. Therefore, R can be written in terms of μ_{RED} and μ_{IR} as shown in Eq. (22). The relations among the various signals are shown in Fig. 6(c-2).

$$R = \frac{\mu_{RED}}{\mu_{IR}} \tag{22}$$

4.2. Calculation of R in the frequency domain

In the method proposed by T. L. Rusch [20], R is calculated from the conventional PPG signal in the frequency domain.

For the case in which two cosine signals are used to drive two light sources of different frequencies, resulting in two PPG AM signals at the light detector. Fig. 6(d-2) shows the PPG AM signals in the frequency domain. To calculate R from the AM magnitude spectra, the AC and DC components, as shown in Fig. 6(d-2) and 6(e-2), are substituted into Eq. (17).

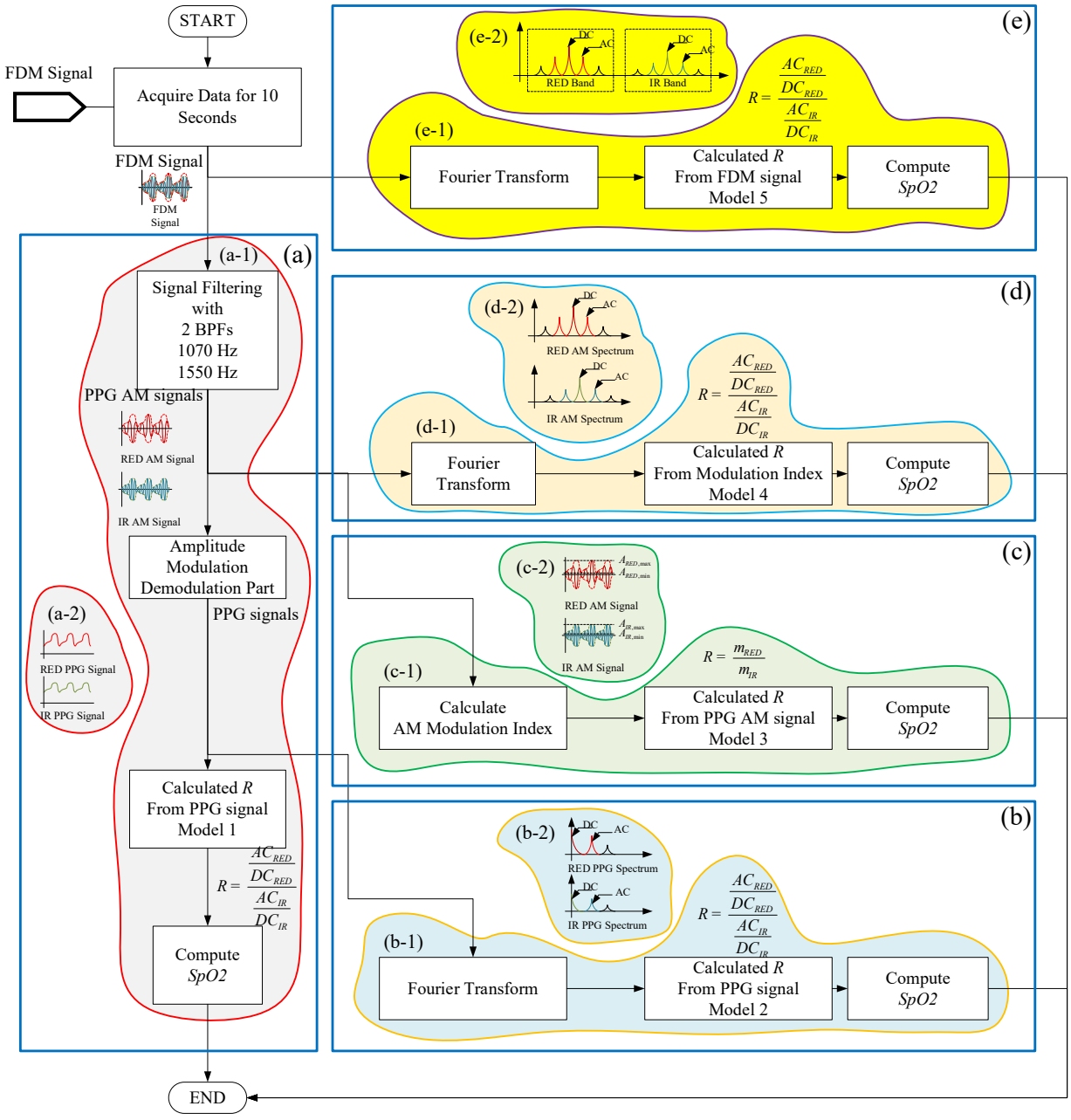

Fig. 6. Signal processing flowchart. (a) Experimental Model 1 is Sakkarin's method [32]. By using BPFs with two different centre frequencies and a corresponding demodulator part, the output signals are obtained as two PPG signals (Fig. 6(a-2)). (b) Experimental Model 2 is Rusche's method [20]. By transforming the PPG signals from Model 1 into the frequency domain, the magnitude spectra of the two PPG signals are obtained. (c) In Experimental Model 3, by filtering the FDM signal with two BPFs, two PPG AM signals are obtained; then, the modulation indexes of these two PPG AM signals are calculated, where μ_{RED} is the modulation index of the red PPG AM signal, while μ_{IR} is the modulation index of the infrared PPG AM signal. (d) In Experimental Model 4, by filtering the FDM signal with two BPFs, two PPG AM signals are obtained; then, these two AM signals are transformed with the FFT. The AC component is the amplitude of the highest peak in the sideband, while the DC component is the amplitude at the carrier frequency. (e) In Experimental Model 5, the FDM signal is transformed directly to obtain its magnitude spectrum, which shows the two bands of the AM signals; then, the AC and DC components can be calculated using the same strategy as in Model 4.

5. System design

The system designed in this article uses two cosine signals of different frequencies to independently drive two light sources: a frequency of 1070 Hz is used to drive the red light source, and a frequency of 1550 Hz is used to drive the infrared light source This system consists of two main components: the analogue front end and the signal processing unit. The analogue front end is shown in Fig. 5. It consists of two oscillator circuits (Fig. 5(a)), light-emitting diode (LED) driver circuits (Fig. 5(b)), a commercial common-anode pulse oximetry probe from Datex-Ohmeda (Fig. 5(c)) and a *trans*-impedance amplifier circuit (Fig. 5 (d)). This analogue front end serves to produce the PPG signals in PPG AM form.

5.1. Cosine oscillator circuit

An XR2206 integrated circuit is used as the sinusoidal oscillator. The output frequency (f) can be calculated from Eq. (23):.

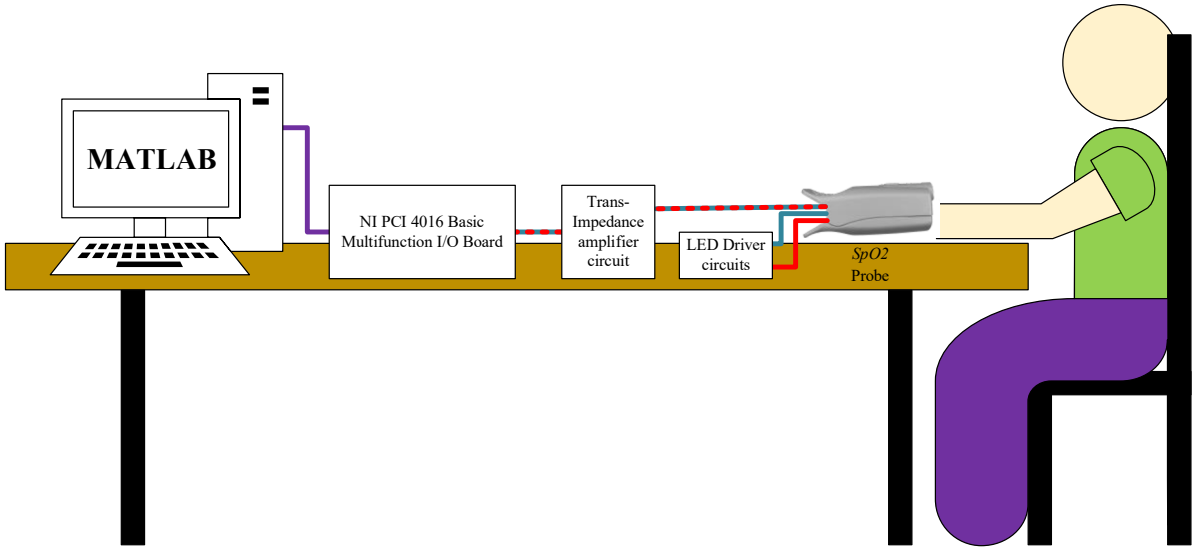

Fig. 7. Experimental setup.

$$f = \frac{1}{RC} \tag{23}$$

For the system considered in this article, the two capacitors c in Fig. 5 (a) are 0.01μF, and the potentiometer R1 is used to adjust the frequencies of the cosine signals, 1070 Hz and 1550 Hz.

5.2. Trans-impedance amplifier circuit

The operational amplifier used in the system presented in this article is an OP07 integrated circuit. As shown in Fig. 5(d), the feedback resistance is $5\,M\Omega$, so the amplifier's gain is 5×10^6 volts per ampere. However, with a feedback capacitor, the amplifier circuit also rejects high frequencies with a cut-off frequency of $3,138$ Hz, acting as a low-pass filter (LPF). The output signal from the *trans*-impedance amplifier circuit is the FDM signal formed by the two PPG AM signals.

5.3. Signal processing

For data acquisition, a NI PCI 4016 Basic Multifunction I/O Board is used to convert the analogue FDM signal into a digital FDM signal at a sampling rate of 16,000 for 10 s. The flow chart of all system operations is shown in Fig. 6. For the study reported in this article, all operations were run in MATLAB software. The FFT function in MATLAB was used to transform the time-domain signals into the frequency domain.

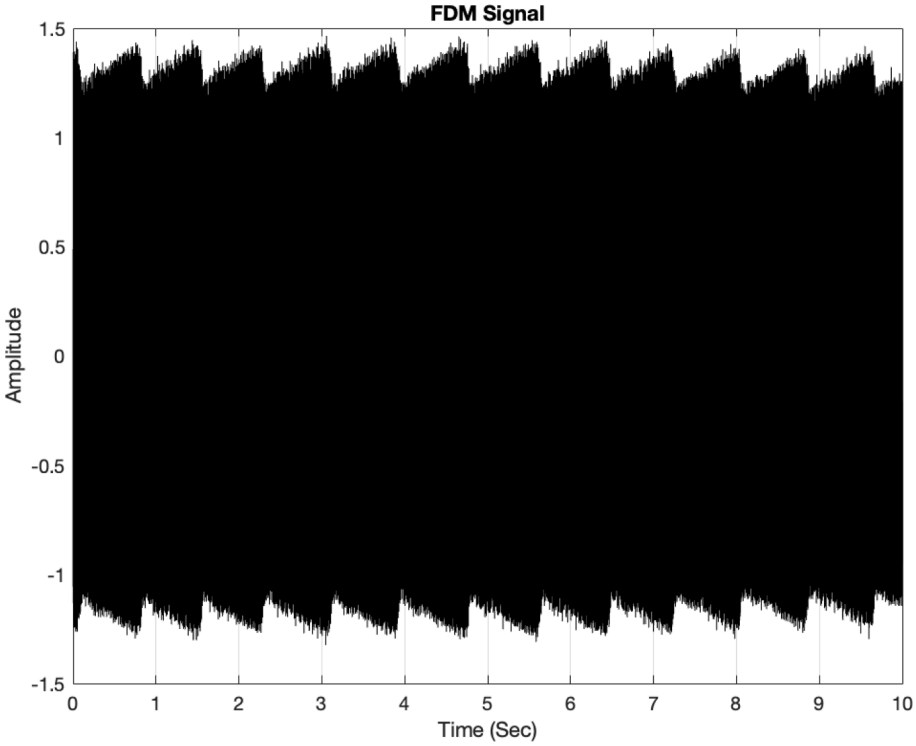

Fig. 8. The FDM signal detected at the light detector. The signal consists of two PPG AM signals: red PPG AM and infrared PPG AM signals.

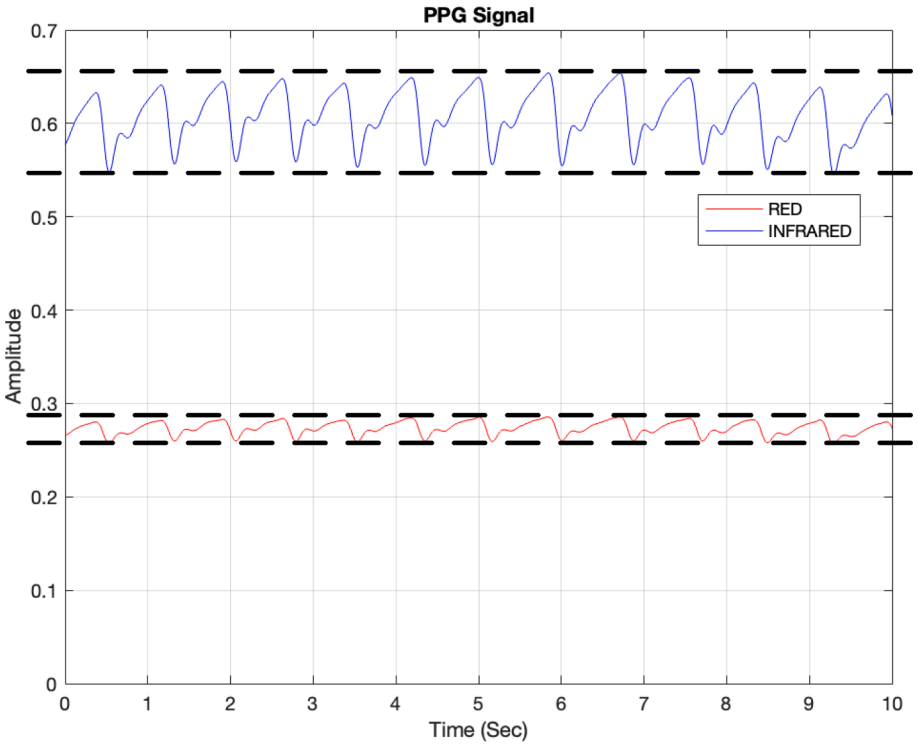

Fig. 9. PPG signals from BPFs and demodulators: (top trace) the infrared PPG signal and (bottom trace) the red PPG signal.

6. Experimental setup

In this article, the experimental setup is shown in Fig. 7. For Fig. 7, The dual light source in the oximeter probe were controlled by two oscillator circuits, and the light detector connected to the *trans*-impedance amplifier circuit to generates the FDM signal and transmitted to the computer (3.40 GHz CPU processor, 4 GB of RAM) by the NI PCI 4016 Basic Multifunction I/O Board and continued processing with MATLAB.

For collecting data, the oximeter probe was attached to volunteer's fingertip. The volunteers were told to sit in relax position, have a minimum movement during the measurement. The experiment was operated in a non-variant ambient light room. The sample signals were acquired from 9 healthy volunteers: 7 male, 2 female, average age is 25 years.

This article has proposed three new models for determining R (The 3rd model (Fig. 6(c)) is time-domain, and the 4th and 5th models (Fig. 6 (d) and 6(e) are frequency domain) and compared them to two traditional methods (The 1st and 2nd models [32,20] (Fig. 6(a) and 6(b)). All the experimental models are shown in Fig. 6. The recorded FDM signal are processed simultaneously. To calculate SpO_2, Eq. (8) is used.

7. Results and discussion

7.1. Frequency-Division multiplexing signal from the light detector

The signal at the detector obtained by driving dual light sources with different cosine signals is shown in Fig. 8.

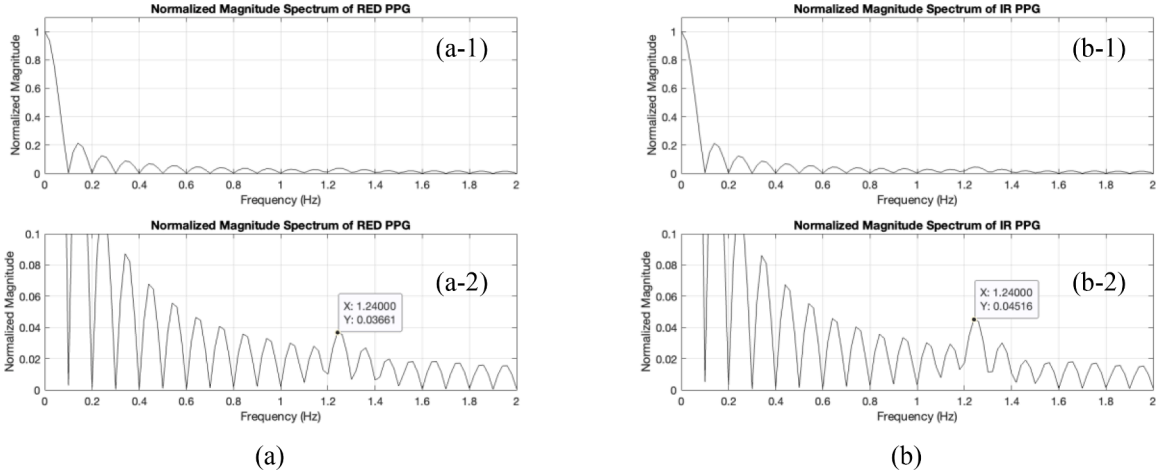

Fig. 10. The normalized magnitude spectrum of the PPG signal (a) The red PPG signal, where (a-1) shows the amplitude of the zero-hertz component and (a-2) shows the amplitude of the cardiac-frequency component. (b) The infrared PPG signal, where (b-1) shows the amplitude of the zero-hertz component and (b-2) shows the amplitude of the cardiac-frequency component.

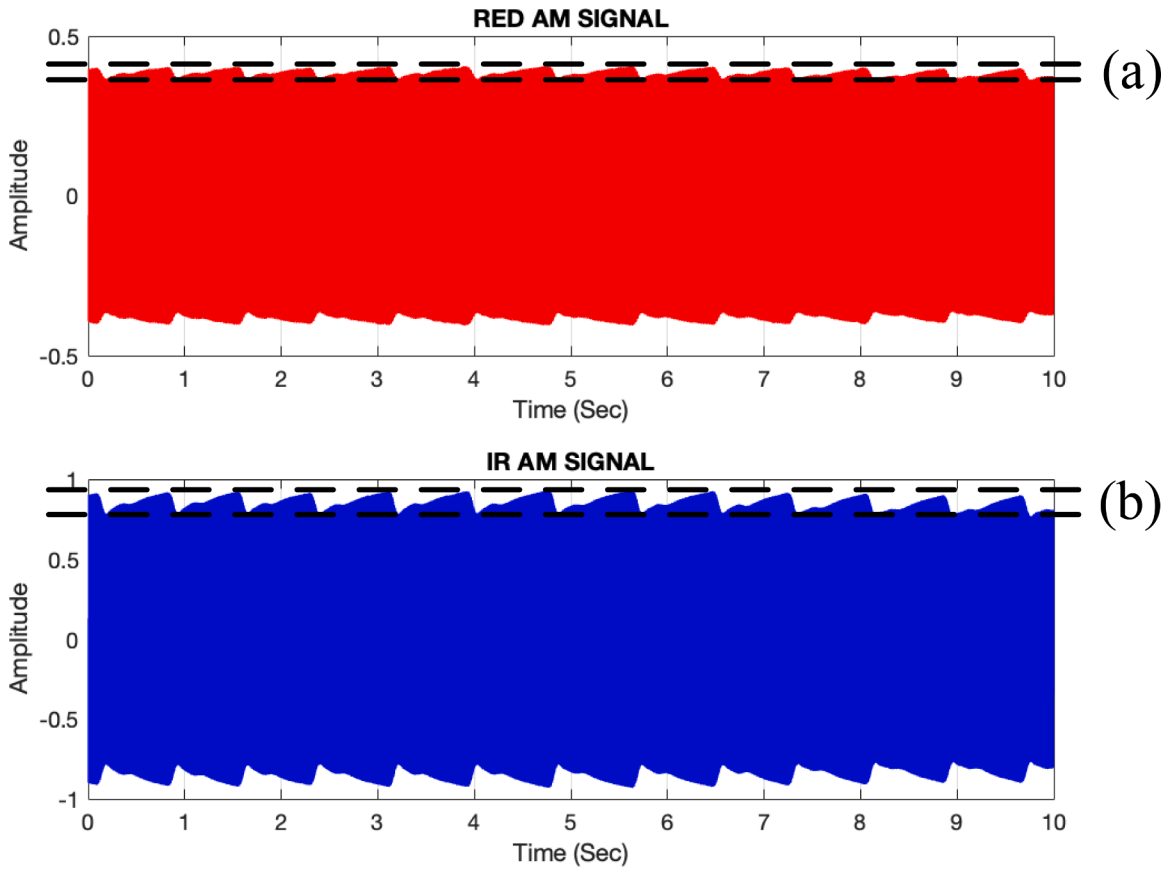

Fig. 11. PPG AM signals. (a) red PPG AM signal with a modulation index of 0.0059 and (b) infrared PPG AM signal with a modulation index of 0.101.

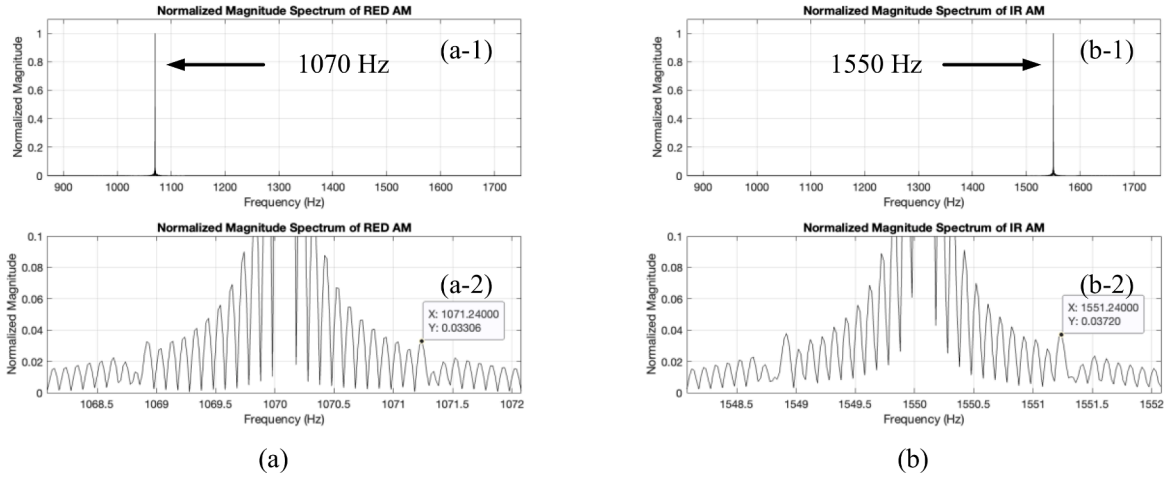

Fig. 12. Normalized magnitude spectrum of the AM PPG signals. (a) red PPG AM signal: (a-1) magnitude of the carrier signal at 1070 Hz and (a-2) expanded to show the shifted cardiac frequency within the 1070 Hz band. (b) infrared AM PPG signal: (b-1) magnitude of the carrier signal at 1550 Hz and (b-2) expanded to show the shifted cardiac frequency within the 1550 Hz band.

7.2. Conventional R calculation

To obtain R, the FDM signal is filtered with two BPFs and demodulators. The PPG signals for the red and infrared light wavelengths are obtained as shown in Fig. 9.

From these PPG signals, Eq. (17) is used to calculate R, and Eq. (8) is used to estimate SpO_2; for Model 1, the R = 0.602 and SpO_2 = 94.92% are achieved. In simultaneous time, the spectrums of the PPG signals in the frequency domain (Model 2), as shown in Fig. 10(a) and (b).

The magnitude of the zero-hertz signal component is the DC component of the PPG signal, and the magnitude of the highest peak at the cardiac frequency is the AC component of the PPG signal. The frequencies of the highest peak magnitudes in Fig. 10(a) and (b) are determined according to the heart rate frequency which is 1.2 Hz and corresponds to a heart rate of 78 beats per minute in Model 1. The R value calculated from the Model 2′s signals in Fig. 10(a) and (b) is R = 0.812, and SpO_2 = 89.40%.

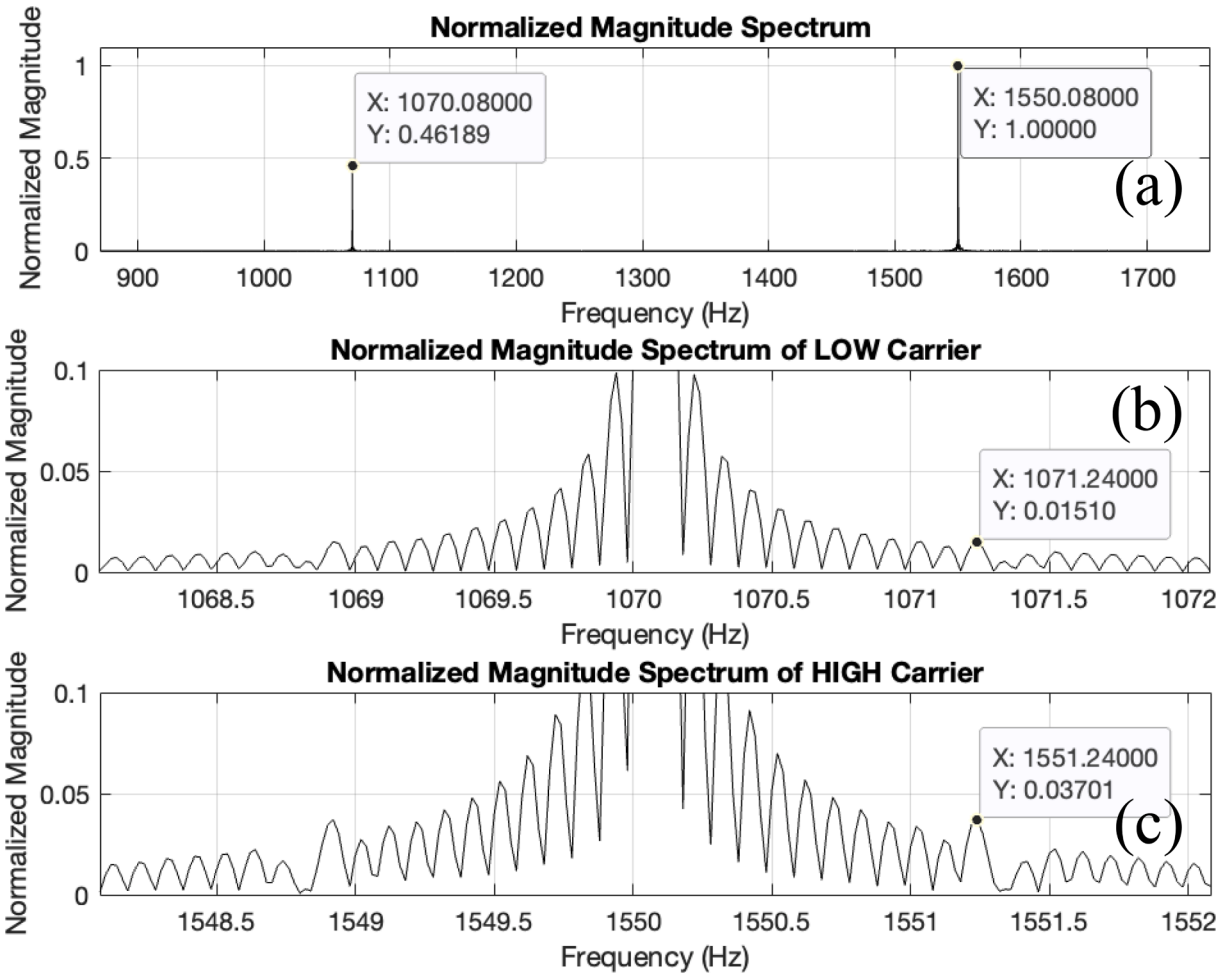

Fig. 13. Normalized magnitude spectrum of the FDM signal: (a) magnitudes of the carrier signals in the 1070 Hz and 1550 Hz bands, (b) expanded to show the shifted cardiac frequency within the 1070 Hz band, and (c) expanded to show the shifted cardiac frequency within the 1550 Hz band.

Table 1
The results of the example signal of 9 volunteers.

Volunteer		Model				
		1	2	3	4	5
1	R	0.5790	0.8569	0.5546	0.8567	0.8588
	SpO_2	95.5257 %	88.5771 %	96.1359 %	88.5817 %	88.5308 %
2	R	0.6050	0.9095	0.5785	0.8427	0.8411
	SpO_2	94.8750 %	87.2618 %	95.5367 %	88.9329 %	88.9735 %
3	R	0.5289	0.8471	0.5266	0.8530	0.8624
	SpO_2	96.7769 %	88.8224 %	96.8359 %	88.6757 %	88.4408 %
4	R	0.6325	0.9268	0.5782	0.9155	0.9018
	SpO_2	94.1884 %	86.8289 %	95.5439 %	87.1114 %	87.4550 %
5	R	0.6152	0.8893	0.5973	0.8987	0.8872
	SpO_2	94.6192 %	87.7664 %	95.0670 %	87.5321 %	87.8191 %
6	R	0.6104	0.8827	0.5709	0.8783	0.8721
	SpO_2	94.7410 %	87.9333 %	95.7280 %	88.0413 %	88.1966 %
7	R	0.5382	0.8454	0.5321	0.8826	0.8659
	SpO_2	96.5457 %	88.8638 %	96.6978 %	87.9351 %	88.3514 %
8	R	0.5956	0.8712	0.5714	0.8849	0.8766
	SpO_2	95.1094 %	88.2209 %	95.7152 %	87.8766 %	88.0851 %
9	R	0.5950	0.8226	0.5809	0.8510	0.8362
	SpO_2	95.1261 %	89.4346 %	95.4764 %	88.7250 %	89.0957 %

7.3. New models for Calculating R

In the time-domain, the PPG AM signals from the BPFs are shown in Fig. 11.

By using Eq. (22) of Model 3 to calculate R in the time domain, the $R = 0.582$ and $SpO_2 = 95.49\%$ are obtained.

While in the frequency-domain, the normalized magnitude spectrum results used to calculate R in the frequency domain in Model 4 are shown in Fig. 12(a) and (b).

The magnitude of the carrier-frequency component is the DC

Table 2
The results of SpO_2 calculated by using Eq. (24) for the frequency domain and using Eq. (8) for the time-domain.

Volunteer		Model				
		1	2	3	4	5
1	R	0.5790	0.8569	0.5546	0.8567	0.8588
	SpO_2	95.5257 %	95.3138 %	96.1359 %	95.3148 %	95.3037 %
2	R	0.6050	0.9095	0.5785	0.8427	0.8411
	SpO_2	94.8750 %	95.0267 %	95.5367 %	95.3915 %	95.4003 %
3	R	0.5289	0.8471	0.5266	0.8530	0.8624
	SpO_2	96.7769 %	95.3674 %	96.8359 %	95.3353 %	95.2841 %
4	R	0.6325	0.9268	0.5782	0.9155	0.9018
	SpO_2	94.1884 %	94.9322 %	95.5438 %	94.9939 %	95.0689 %
5	R	0.6152	0.8893	0.5973	0.8987	0.8872
	SpO_2	94.6192 %	95.1368 %	95.0670 %	95.0857 %	95.1484 %
6	R	0.6104	0.8827	0.5709	0.8783	0.8721
	SpO_2	94.7410 %	95.1733 %	95.7280 %	95.1969 %	95.2308 %
7	R	0.5382	0.8454	0.5321	0.8826	0.8659
	SpO_2	96.5457 %	95.3764 %	96.6978 %	95.1737 %	95.2646 %
8	R	0.5956	0.8712	0.5714	0.8849	0.8766
	SpO_2	95.1094 %	95.2361 %	95.7152 %	95.1609 %	95.2064 %
9	R	0.5950	0.8226	0.5809	0.8510	0.8362
	SpO_2	95.1261 %	95.5010 %	95.4764 %	95.3461 %	95.4270 %

component of the PPG signal, and the magnitude of the highest peak in each sideband is the AC component. From Fig. 12(a) and (b), R = 0.89 can be calculated and SpO_2 = 87.70% is estimated. Moreover, these plots show how the signal modulation moves the PPG signals from low frequency (0 – 2 Hz) to high frequency (LSB or USB).

Finally, the FDM signal in the frequency domain is shown in Fig. 13. For Model 5, the R calculation is similar to that in Model 4; the difference is that the red and infrared PPG AM signals whose spectra are used in Model 4 are physically separated by BPFs, while the signals whose spectra are used in Model 5 are not physically separated. Model 5 yields R = 0.88 and an estimate of SpO_2 = 87.91%.

7.4. New equation for estimating SpO_2 in the frequency domain

Based on the results of calculating SpO_2 using Eq. (8) from all volunteers' data, the light absorbance ratio and SpO_2 are shown in Table 1.

From Table 1 of 9 volunteers, it shown that the light absorbance ratio of the 5 experimental models is different, its cause of difference SpO_2, because using the Eq. (8) to calculate SpO_2 which this equation corresponds to the time-domain method. So, the frequency-domain group incurs more error because in the frequency domain, the only part of the AC component that is used is the part at the fundamental cardiac frequency or the first peak in the sideband (the first peak in the sideband corresponds to the fundamental cardiac frequency after being shifted from the low-frequency region). For greater accuracy, the harmonic frequencies of the fundamental cardiac frequency should all be used in the calculation; however, estimating the AC component with more harmonic frequencies is more complex because not only the amplitudes of the harmonic frequencies but also their phase responses must be calculated. However, the R values calculated using Models 2, 4, and 5 are all very similar; therefore, to achieve greater accuracy, a new mathematical model for evaluating SpO_2 based on R as calculated in the frequency domain (R_{Freq}) is introduced in Eq. (24):.

$$SpO_2|_{Freq} = 99.99 - 5.457R_{Freq} \tag{24}$$

where $SpO_2|_{Freq}$ is the blood oxygen saturation derived from the frequency domain. Which this expression is determined by using the linear regression of R_{Freq} (the light absorbance ratio in the frequency-domain) and SpO_2 in the time domain of the Model 1 (conventional method).

When Eq. (24) is used to calculate the SpO_2 in the frequency-domain, it gave the results as shown in Table 2.

From Table 2 of 9 volunteers, it shown that the light absorbance ratio of the 5 experimental models is different, but the SpO_2 is almost the same, because the experiment models 2, 4, and 5 used the new equation for approximate SpO_2 in the frequency-domain, and the errors of SpO_2 are shown in Table 3.

Table 3
Average Errors and Variances Using Eqs. (8) and (24).

Model	Equation (8)		Equation (24)	
	Average SpO_2 error	Variance	Average SpO_2 error	Variance
2	6.2927	39.5984	1.0353	1.0719
3	0.7138	0.5095	0.7138	0.5095
4	7.87	61.9369	1.0279	1.0566
5	7.7758	60.4630	1.0760	1.1578

In Table 3, the SpO_2 results obtained by using Eq. (24) and Eq. (8) which is estimated from R in the frequency-domain. It shown that estimated SpO_2 from Eq. (24) are more accurate than using Eq. (8). Thus, it is demonstrated that eventually to estimate SpO_2 from the FDM signal in the frequency-domain, the system does not need to be demodulated and including the use of the BPFs to separate the signal, but it can be obtained directly from the magnitude spectrum of the FDM signal, thereby reducing the overall complexity of the overall processing system.

8. Conclusion

The results of the five models are shown in Figs. 9–13, and the calculated errors are shown in Table 3. The error results can be divided into two groups: a time-domain group and a frequency-domain group. The SpO_2 errors are larger in the frequency-domain group than in the time-domain group because of the treatment of the AC component. In the frequency-domain group, only the fundamental cardiac frequency is considered in the AC component; achieving greater accuracy would require increased complexity because it would be necessary to use more harmonic frequencies of the fundamental cardiac frequency. In this case, not only the amplitudes of the harmonics but also their phases would need to be determined. Therefore, a new mathematical model for estimating blood oxygen saturation in the frequency domain is proposed in Eq. (24). When Eq. (24) is used to calculate SpO_2 based on the R-value calculated in the frequency domain, the error drops to 1%. The results show that with the new methods for calculating R using the modulation indexes, corresponding to Models 3 and 4, demodulators are unnecessary, and eventually, with Model 5, there is also no need for BPFs. With no demodulators and BPFs in Model 5, the analogue front-end design is simpler, also the signal processing. Finally, for Models 1, 2, 3, and 4, which used the BPFs, the wavelet base technique for separate PPG AM signals can be substitute to the BPFs.

CRediT authorship contribution statement

Pattana Kainan: Methodology, Software, Writing – original draft. **Ananta Sinchai:** Software, Investigation, Writing – review & editing. **Panwit Tuwanut:** Investigation, Writing – review & editing. **Paramote Wardkein:** Supervision, Conceptualization.

Declaration of Competing Interest

The authors declare that they have no known competing financial interests or personal relationships that could have appeared to influence the work reported in this paper.

Acknowledgement

This research did not receive any specific grant from funding agencies in the public, commercial, or not-for-profit sectors.

References

[1] J.F. Biebuyck, J.W. Severinghaus, J.F. Kelleher, Recent Developments in Pulse Oximetry, Anesthesiology. 76 (1992) 1018–1038, https://doi.org/10.1097/00000542-199206000-00024.
[2] S. DeMeulenaere, Pulse Oximetry: Uses and Limitations, J. Nurse Pract. 3 (2007) 312–317, https://doi.org/10.1016/j.nurpra.2007.02.021.
[3] M. Nitzan, A. Romem, R. Koppel, Pulse oximetry: fundamentals and technology update, Med Devices (Auckl). 7 (2014) 231–239, https://doi.org/10.2147/MDER.S47319.
[4] S. Seifi, A. Khatony, G. Moradi, A. Abdi, F. Najafi, Accuracy of pulse oximetry in detection of oxygen saturation in patients admitted to the intensive care unit of heart surgery: comparison of finger, toe, forehead and earlobe probes, BMC Nurs. 17 (2018) 17, https://doi.org/10.1186/s12912-018-0283-1.
[5] A. Jubran, Pulse oximetry, Crit Care. 3 (1999) R11–R17, https://doi.org/10.1186/cc341.
[6] O. Wieben, Light Absorbance in Pulse Oximetry, in: J.G. Webster (Ed.), Design of Pulse Oximeters, Taylor & Francis, USA, New York, 1997, pp. 40–55.
[7] M.W. Wukitsch, M.T. Petterson, D.R. Tobler, J.A. Pologe, Pulse oximetry: analysis of theory, technology, and practice, J. Clin. Monit. 4 (1988) 290–330, https://doi.org/10.1007/BF01617328.
[8] J. Farmer, Blood Oxygen Measurement, in: J.G. Webster (Ed.), Design of Pulse Oximeters, Taylor & Francis, USA, New York, 1997, pp. 21–39.
[9] J.-A. Collins, A. Rudenski, J. Gibson, L. Howard, R. O'Driscoll, A, Rudenski A, Gibson J, Howard L, O'Driscoll R, Relating oxygen partial pressure, saturation and content: the haemoglobin-oxygen dissociation curve, Breathe (Sheff). 11 (3) (2015) 194–201.
[10] J. Sendroy, Manometric determination of hemoglobin by oxygen capacity method, J. Biol. Chem. 91 (1931) 307–323, https://doi.org/10.1016/S0021-9258(18)76615-5.
[11] Y. Mendelson, Pulse oximetry: theory and applications for noninvasive monitoring, Clin. Chem. 38 (9) (1992) 1601–1607.
[12] C. Wang, K. Tang, Active noise cancellation of motion artifacts in pulse oximetry using isobestic wavelength light source, 2011 IEEE International Symposium of Circuits and Systems (ISCAS). Rio de Janeiro. (2011) pp. 1029-1032. https://doi.org/10.1109/ISCAS.2011.5937744.
[13] Y. Pole, Evolution of the pulse oximeter, Int. Congress Series. 1242 (2002) 137–144.
[14] J.F. Kelleher, Pulse oximetry, J. Clin. Monit. 5 (1989) 37–62, https://doi.org/10.1007/BF01618369.
[15] E. James, Sinex, Pulse oximetry: Principles and limitations, Am. J. Emergency Med. 17 (1) (1999) 59–66.
[16] Gibbs Peter, Wood Levi. Asada Harry, Active motion artifact cancellation for wearable health monitoring sensors using collocated MEMS accelerometers, Proceedings of SPIE - The International Society for Optical Engineering. (2005). https://doi.org/5765.10.1117/12.600781.
[17] S. Ardalan, S. Moghadami, S. Jaafari, Motion Noise Cancelation in Heartbeat Sensing using Accelerometer and Adaptive Filter, IEEE Embedded Systems Letters. 7 (4) (2015) 101–104, https://doi.org/10.1109/LES.2015.2457933.
[18] A.R. Relente, L.G. Sison, Characterization and adaptive filtering of motion artifacts in pulse oximetry using accelerometers, Proceedings of the Second Joint 24th. (2002) 1769–1770. https://doi.org10.1109/IEMBS.2002.1106644.
[19] K.A. Reddy, B. George, V.J. Kumar, Motion Artifact Reduction and Data Compression of Photoplethysmo-graphic Signals utilizing Cycle by Cycle Fourier Series Analysis, 2008 IEEE Instrumentation and Measurement Technology Conference. (2008) 176–179, https://doi.org/10.1109/IMTC.2008.4547026.
[20] T.L. Rusch, R. Sankar, J.E. Scharf, Signal processing methods for pulse oximetry, Comput. Biol. Med. 26 (2) (1996) 143–159.
[21] J.M. Kim, S.H. Kim, D.J. Lee, H.S. Lim, Signal processing using Fourier & wavelet transform for pulse oximetry, Technical Digest. CLEO/Pacific Rim 2001. 4th Pacific Rim Conference on Lasers and Electro-Optics (Cat. No.01TH8557) (2001) 310–311. https://doi.org/10.1109/CLEOPR.2001.970957.
[22] F. Peng, Z. Zhang, X. Gou, H. Liu, W. Wang, Motion artifact removal from photoplethysmographic signals by combining temporally constrained independent component analysis and adaptive filter, BioMed Eng. OnLine 13 (1) (2014).
[23] K.W. Chan, Y.T. Zhang, Adaptive reduction of motion artifact from photoplethysmographic recordings using a variable step-size LMS filter, SENSORS, IEEE. 2 (2002) (2002) 1343–1346, https://doi.org/10.1109/ICSENS.2002.1037314.
[24] M.R. Ram, K.V. Madhav, E.H. Krishna, N.R. Komalla, K.A. Reddy, A Novel Approach for Motion Artifact Reduction in PPG Signals Based on AS-LMS Adaptive Filter, IEEE Trans. Instrum. Meas. 61 (5) (2012) 1445–1457.
[25] B.S. Kim, S.K. Yoo, Motion artifact reduction in photoplethysmography using independent component analysis, IEEE Trans. Biomed. Eng. 53 (3) (2006) 566–568, https://doi.org/10.1109/TBME.2005.869784.
[26] K.A. Reddy, V.J. Kumar, Motion Artifact Reduction in Photoplethysmographic Signals using Singular Value Decomposition, 2007 IEEE Instrumentation & Measurement Technology Conference (IMTC 2007). (2007) 1–4. https://doi.org/10.1109/IMTC.2007.379467.
[27] R.W.C.G.R. Wijshoff, M. Mischi, R.M. Aarts, Reduction of periodic motion artifacts in photoplethysmography, IEEE Trans. Biomed. Eng. 64 (1) (2017) 196–207, https://doi.org/10.1109/TBME.2016.2553060.
[28] S. Chugh, A. Akula, Effect of Different Signal Processing Techniques on a Calibration Free Pulse Oximeter, 2018 3rd International Conference for Convergence in Technology (I2CT). (2018) 1–6. https://doi.org10.1109/I2CT.2018.8529537.
[29] J. Harvey, S.M.A. Salehizadeh, Y. Mendelson, K.H. Chon, OxiMA: A Frequency-Domain Approach to Address Motion Artifacts in Photoplethysmograms for Improved Estimation of Arterial Oxygen Saturation and Pulse Rate, IEEE IEEE Trans. Biomed. Eng. 66 (2) (2019) 311–318, https://doi.org/10.1109/TBME.2018.2837499.
[30] P.J. Chacon, L. Pu, T.H. da Costa, Y.-H. Shin, T. Ghomian, H. Shamkhalichenar, H.-C. Wu, B.A. Irving, J.-W. Choi, A Wearable pulse oximeter with wireless communication and motion artifact tailoring for continuous use, IEEE IEEE Trans. Biomed. Eng. 66 (6) (2019) 1505–1513.
[31] James Patterson, A Photoplethysmography System Optimised for Pervasive Cardiac Monitoring, PhD Thesis, Imperial College London, England, 2013. https://doi.org/10.25560/11110.
[32] S. Sinchai, P. Kainan, P. Wardkein, J. Koseeyaporn, A Photoplethysmographic signal isolated from an additive motion artifact by frequency translation, IEEE Trans. Biomed. Circuits and Syst. 12 (4) (2018) 904–917, https://doi.org/10.1109/TBCAS.2018.2829708.
[33] J. Koseeyaporn, S. Sinchai, P. Wardkein, Performance of Frequency Translation in Separating a Photoplethysmographic Signal from an Additive Motion Artifact, in: 2019 IEEE 4th International Conference on Computer and Communication Systems (ICCCS), 2019, pp. 512–516.
[34] J.G. Webster, Design of Pulse Oximeters, 1st ed., Taylor & Francis, New York, USA, 1997.